Proceedings of the ASME 2010 3rd Joint US-European Fluids Engineering Summer Meeting and 8th International Conference on Nanochannels, Microchannels, and Minichannels
FEDSM-ICNMM2010
August 1-5, 2010, Montreal, Canada

FEDSM-ICNMM2010-30546

NUMERICAL SIMULATIONS OF THE INTRA-ANEURYSMAL VORTEX SHEDDING IN INDUCED MOUSE ABDOMINAL AORTIC ANEURYSMS

Matthew D. Ford*
Ugo Piomelli
Department of Mechanical and Materials Engineering
Queen's University
Kingston, Ontario Canada
Email: matthew.david.ford@gmail.com

Richard Y. Cao
Department of Physiology
Queen's University
Kingston, Ontario Canada

Colin D. Funk
Departments of Physiology and Biochemistry
Queen's University
Kingston, Ontario Canada

Andrew Pollard
Department of Mechanical and Materials Engineering
Queen's University
Kingston, Ontario Canada

ABSTRACT

A feature of particular interest observed in vivo in murine abdominal aortic aneurysm (AAA) is the presence of a vortex shed from the proximal edge of the abdominal aortic aneurysm. It is unclear whether the occurrence of the shed vortex is due to the periodic nature of the flow-rate waveform, to geometric features, or to the compliant nature of the vessel tissue. Numerical simulations were performed on 3D semi-idealized and 2D axi-symmetric models of the abdominal aortic aneurysm at a mean Reynolds number of 63 and a Womersley number of 2 (for unsteady inflow conditions). The numerical results from the 3D model showed good agreement with the flows visualized by Doppler Ultrasound with respect to the development of the observed shed vortex. The idealized axi-symmetric models under steady flow conditions showed no signs of vortex shedding. Under unsteady inflow conditions, however, shear-layer roll-up occurred near the peak systolic velocity. The presence of a proximal lip was found to lead to vortex separation (from the wall) earlier in the cardiac cycle, and the presence of the proximal narrowing led to the earliest vortex separation. The sensitivity to the inflow waveform shape also showed that the presence of the shedding, in the model with proximal narrowing, disappeared when the peak-to-mean velocity ratio was reduced by approximately half. Therefore, we conclude that the observed intra-aneurysmal vortex shedding is a shear-layer rollup phenomenon; however, the geometry can act to enhance further the observed vortex shedding.

INTRODUCTION

An abdominal aortic aneurysm (AAA) is a dilation of at least 1.5 times the diameter of the largest blood vessel [1]. These dilations are characterized by discrete structural deterioration of the aortic wall, and occur in up to 10% of the population greater than 65 years of age, with preponderance in males [1–6]. They often progress slowly over many years, but eventually rupture; abdominal aortic aneurysms (AAAs) are estimated to be the 10th most common cause of mortality and are responsible for 2% of all deaths in developed countries [4]. AAAs exhibit many features of inflammation and tissue degeneration that are common

*Address all correspondence to this author.

to chronic diseases [5]. Smoking and hypertension are prime risk factors for AAA, combined with inflammatory processes in the vessel wall that includes atherosclerotic plaque buildup. Remodeleing events in the vessel wall are exacerbated by alterations in mechanical forces that change over time [7]. These events disrupt the extracellular matrix resulting in altered collagen and elastin, adaptive remodeling and smooth muscle cell depletion.

There is a dearth of knowledge as to the molecular and cellular events that cause the development of human AAAs [2–5] because most of our information is gleaned from pathological specimens obtained at the time of surgical intervention or at autopsy. To circumvent this drawback, several rodent models of AAA have been developed either via genetic exploitation or via chemical methods; their advantages and limitations have been considered [8]. The angiotensin II (AngII) infusion mouse model in the atherosclerotic susceptible strain (apolipoprotein E deficient) has become the most widely used model in recent years because of its simplicity and because certain facets of the model resemble human disease acquisition, including male gender preponderance in the setting of mild hypertension with enhanced incidence in the presence of hyperlipidemia [8, 9]. There is a well-defined time course of events in this model with early macrophage infiltration into the smooth muscle-rich medial layer of the aneurysm-prone area, transmedial dissection that causes rapid luminal expansion within the first 7 days of AngII infusion, with subsequent complex inflammatory events that include intramural thrombus formation, elastin degradation and profound remodeling in which the thrombus is often resorbed and replaced by fibrous tissue interspersed with leukocytes [9, 10].

There has been much work describing the fluid dynamical environment within a human AAA [11–16], but with the considerable research being undertaken with the AAA mouse model it is important to understand this unique hemodynamic environment and how it may be different from that of the human. Within the range of human flow conditions using idealized aneurysm geometries previous studies have quantified the dominant flow features. Yu *et al*. [11] observed the presence of a single large vortex in the aneurysm bulb under steady flow conditions; the vortex shifted towards the distal end of the aneurysm as the Reynolds number (*Re*) (based on the normal vessel diameter and the mean velocity over the cardiac cycle) was increased from 400 to 1400. With unsteady inflow conditions driven by a sine wave, they observed migration of this vortex from the proximal to the distal end of the aneurysm bulb during the systolic deceleration phase of the flow cycle. Taylor *et al*. [13] also report a similar finding in their computational study of side wall AAA models, with a vortex being formed at the proximal edge of the aneurysm just after peak systole and traveling the length of the aneurysm during the systolic deceleration. Yip *et al*. [12] demonstrated, using particle flow visualization, the presence of vortex separation at $Re = 445$ and Womersley number (dimensionless number describing the ratio of the frequency of the flow-rate waveform to the viscous effects) of ($\alpha = 7.3$). The vortices formed on the proximal wall during systolic acceleration, but did not separate until early diastole. Sheard *et al*. [14] studied the flow in an idealized axisymmetric AAA model at $Re = 330$ and $\alpha = 10.3$, again observing vortex formation and separation during the systolic deceleration phase of the cardiac cycle. Finol *et al*. [15] studied the flow in asymmetric idealized models of human AAA at $Re = 300$ and $\alpha = 11.5$. They found, similarly, that vortices were formed and shed from the proximal edge of the aneurysm during the systolic deceleration phase of the cardiac cycle. There has also been much work studying the patient specific flow patterns of the human geometries [17–19] .

In a first attempt to understand the intra-aneurysmal fluid dynamics of mouse AAA we focus, in this study, on the mechanisms by which unsteady flow patterns originate; that were observed by Doppler ultrasound ECG-based Kilohertz Visualization (DUS-EKV) . To this end the flow patterns were first reproduced by means of a semi-idealized three-dimensional model of the mouse AAA. To elucidate further the parameter space under which this observed unsteadiness occurs, a series of idealized axi-symmetric models with different inlet flow conditions were explored.

METHODS

In vivo studies of AAA induction were performed in mice, which were of an apolipoprotein E (apoE) deficient genetic background and male in gender. Alzet osmotic mini-pumps loaded with angiotensin II (Ang II) were implanted subcutaneously into mice (8-12 weeks of age) in the dorsal region under isoflurane anesthesia to obtain a delivery rate of 1 $\mu g/kg/min$ over the course of 4 weeks. An AAA was defined as having a minimum of 150% enlargement of the diameter of the aorta. Abdominal aortic enlargements, as well as aneurysm complications such as aortic dissection and rupture were observed during the study. The Animal Use Committee at Queens University approved all animal protocols.

Ultrasound Imaging was performed with mice placed supine on a heated table under isoflurane anesthesia and depilated with hair removal cream. A Vevo 770 high-resolution ultrasound imaging system (VisualSonics, Toronto, Canada) with 40 MHz frequency real-time microvisualization scan-head (RMV 704) and 10 x 10 mm field of view was used first in B-mode to obtain a 2D transverse image to localize the suprarenal abdominal aorta on day 7 post-Ang II infusion. Aortas were then visualized longitudinally via B-mode imaging and confirmed by Pulsed-wave Doppler. A more detailed examination of complex fluid-dynamical changes during AAA formation was obtained by the ECG-based Kilohertz Visualization (EKV) reconstruction technique that synthesizes B-mode images from a series of heart rhythm cycles and reconstructs one representative heart cycle that is spatially precise and synchronized to the animals ECG (VisualSonics soft-

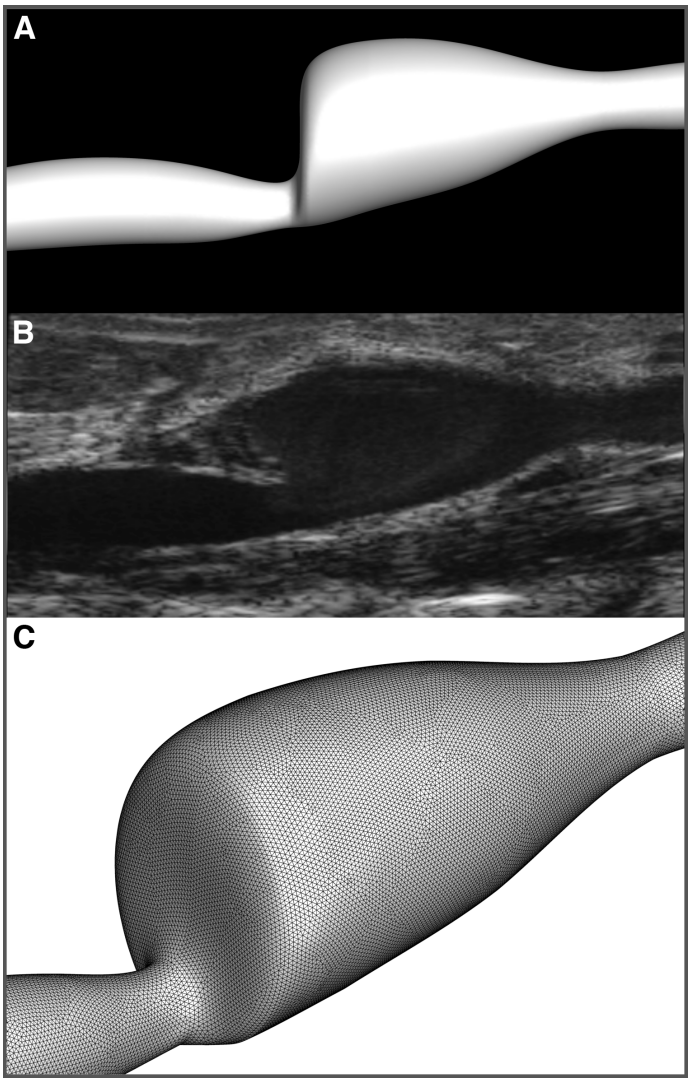

FIGURE 1. (A) LATERAL VIEW OF THE SEMI-IDEALIZED COMPUTATIONAL MOUSE MODEL. (B) DUS IMAGE ON WHICH THE DIMENSIONS OF THE COMPUTATIONAL MODEL (A) WERE BASED. (C) 45° VIEW HIGHLIGHTING THE ASSUMED CIRCULAR CROSS SECTION ALONG WITH THE TETRAHEDRAL SURFACE MESH.

ware). Recorded EKV Cine Loop videos (120 frames at a rate of 1000 Hz) were further analyzed, measured, annotated and reconstructed into computerized models to elucidate the mechanism of observed vortex shedding during AAA formation. Power Doppler 3D acquisitions were initially conducted on day 14 and 28 to obtain parameters of 3D geometry and volume changes to be followed up after analysis of all initial samples with a new set of animals at day 7. Twenty-one mice with AAAs were imaged over the 4-week course of the study. Mice with ruptured aneurysms were not included in these numbers.

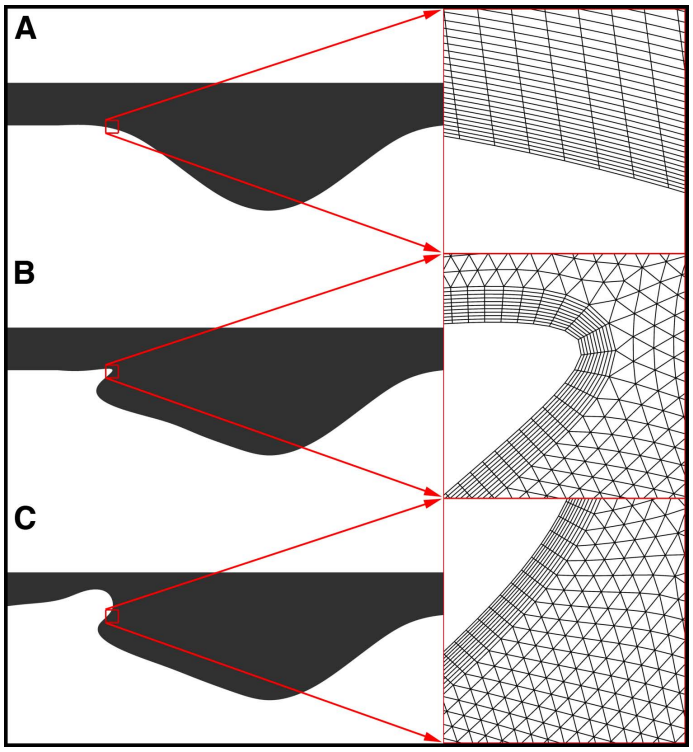

FIGURE 2. (A) AXI-SYMMETRIC MODEL BASED ON YIP *et al*. [12]. THE AXI-SYMMETRIC MODEL WAS SUBSEQUENTLY ALTERED TO INCLUDE A PROXIMAL LIP (B) AND 50% NARROWING (C). NOTE THE ZOOMED IN REGIONS HIGHLIGHTING THE MESH DENSITY IN THE CRITICAL SEPARATION REGION.

Safety concerns for the mice, related to the length of time under anesthetic, made it unfeasible to acquire a 3D image data set and an EKV flow image within the same week. In this study 3D images were only acquired one week following the EKV velocity measurements. Rapid remodeling of the intra luminal region occurred during the week between the EKV and the 3D image data collection. Therefore, the 3D image data were not a reliable model of the 3D geometry during the time of the EKV-DUS flow visualization. To facilitate our understanding of the mouse AAA hemodynamics a semi-idealized model (Figure 1A) was constructed based on the reconstructed B-mode image. This was accomplished by measuring the lumen diameter at various locations along the axial length. As no out-of-plane information was available the simplifying assumption was made that the cross section of the vessel was circular. This produced a model that was anatomically realistic in one plane of view but idealized by the assumption of a circular cross-section. Upstream of the inlet and downstream of the outlet flow extensions of length ten times the inlet cross sectional diameter were appended to minimize end effects. The tubular inlet and outlet sections of the model were meshed using hexahedral elements while the more

geometrically complex aneurysm section was meshed with tetrahedral elements. In total the model is comprised of 771,000 elements with 572,000 of the elements in the area of the vessel narrowing and aneurysm bulge.

Three idealized axi-symmetric models were constructed to further explore the parameter space under which the observed vortex shedding was occurring. The idealized aneurysm geometry was based on the geometry characterized by Yip *et al*. [12] with a peak height of twice the vessel diameter and an aneurysm length of five times the vessel diameter (Figure 2A). This model was subsequently altered to create a second model with a lip at the aneurysms proximal edge (Figure 2B) and a third model with a proximal-aneurysmal narrowing of one half the vessels original diameter (Figure 2C). Each of the three models had added to it a five-diameter-long inlet section and twenty-diameter-long outlet section, to insure fully developed flow entering the aneurysm section and remove outflow boundary condition interference. The idealized model based on the geometry of Yip *et al*. [12] was meshed with 105,000 hexahedral elements. The inlet and outlet extension sections of the modified geometries, lip and proximal narrowing, were meshed with hexahedral elements while the aneurysm portion of the geometry was meshed with tetrahedral elements for a total of 78,000 and 81,000 elements respectively.

All simulations were performed using the unstructured finite-volume solver, openFOAM® [22], which is second-order accurate in time and space. In this study we have assumed smooth walls and Newtonian fluid. As the inlet flow-rate waveform was not measured for the mouse, on which the 3D model was based, we applied the mean suprarenal waveform measured by Amirbekian *et al*. [20]. Based on this work a mean Reynolds number of 63 and a Womersley number of 2 were prescribed as the working parameters (for unsteady inflow conditions). At the inlet a fully developed Womersley velocity profile [23] was applied (in the case of steady flow a fully developed Poiseuille profile was used at the inlet) and a homogenous Neuman condition for pressure. At the outlet the homogenous Neuman condition was applied for velocity and a fixed value of pressure. Since the flow is laminar (although unsteady) no turbulence model is required.

The first goal of this study was to explore, using computational fluid dynamics (CFD), the vortex shedding observed via EKV Doppler ultrasound in more detail, as the flow visualization technique relies on averaging images taken over multiple cardiac cycles. The general flow patterns observed in the 3D mouse model were also of great interest as, to the authors knowledge, these flow patterns have not yet been reported in the literature. To further understand the role of geometry, three axi-symmetric models were incorporated, from the simple one to models containing geometrical characteristics expected to enhance shedding. Finally we also wished to explore the role the inlet flow rate waveform had on the observed shedding. To this end, aside from the normal mouse suprarenal waveform [20], steady flow, a sine-wave driven flow and a flow driven by an average human carotid artery waveform [21] were used as inlet flow boundary condititions (all scaled to the Reynolds and Womersley number of the mouse).

RESULTS

As the mouse model is currently being used as a surrogate for the human aneurysm, it is imperative that we understand the fluid mechanic environment in the mouse and how it relates to that of the human. Unsteady flow patterns were observed, to some degree, in eleven of the fifteen mice that underwent full EKV Cine Loop scanning. The observed vortex shedding is characterized by the formation of a small vortex at the proximal edge of the aneurysm (Figure 3A, B), which then detaches and travels the length of the aneurysm (Figure 3C - F). The time frame over which this shedding occurs is less then 1/15 of the cardiac cycle. Although the DUS-EKV images were not registered to the flow rate waveform, it appears from the animations that the shedding is occurring as the flow accelerates towards the peak systolic value, this is one of the questions we wish to clarify with our computational models. This process can be seen even more clearly in a second mouse, on which the semi-idealized 3D model was based, in Figure 4 (right-hand column).

The 3D model shows qualitative agreement with the DUS visualization (Figure 4), with A high degree of similarity observed in both the position and size of the vortex at each point in the cardiac cycle (Figure 4). From the semi-idealized model we can see that the vortex shedding is initiated as the flow accelerates towards the peak systolic value (Figure 4, inset waveforms), it appears as though the vortex is riding on the front of the accelerating fluid as it moves through the aneurysm domain; after it reaches the distal side of the aneurysm a stable vortex is established within the aneurysm, which migrates to the proximal end of the aneurysm for the remainder of the cardiac cycle. Here we postulate that the shed vortex is caused by a rollup of the shear-layer, as the jet of fluid accelerates through the aneurysm cavity, while prior to systolic acceleration the fluid in the suprarenal abdominal aorta is moving with a velocity very close to zero.

To further understand if this shear-layer rollup is driven by the sharp proximal edge or the presence of the proximal narrowing to the aneurysm, a series of three idealized aneurysms were explored (Figure 2). First note that for all three models the flow within the aneurysm bulb both prior to and following the shed vortex (Figure 5, top and bottom row respectively) is driven by a single large vortex (aside from the case of the proximal narrowing, which shows a secondary vortex at the aneurysm dome during deceleration most likely caused by the increased momentum imparted to the large circulation by the presence of the proximal narrowing). All three models show vortex shedding originating off of the proximal wall of the aneurysm during the systolic acceleration (Figure 5, middle row). Note however that the lip caused the separation to occur at an earlier stage in systolic acceleration then that of the model based on Yip *et al*. [12] and,

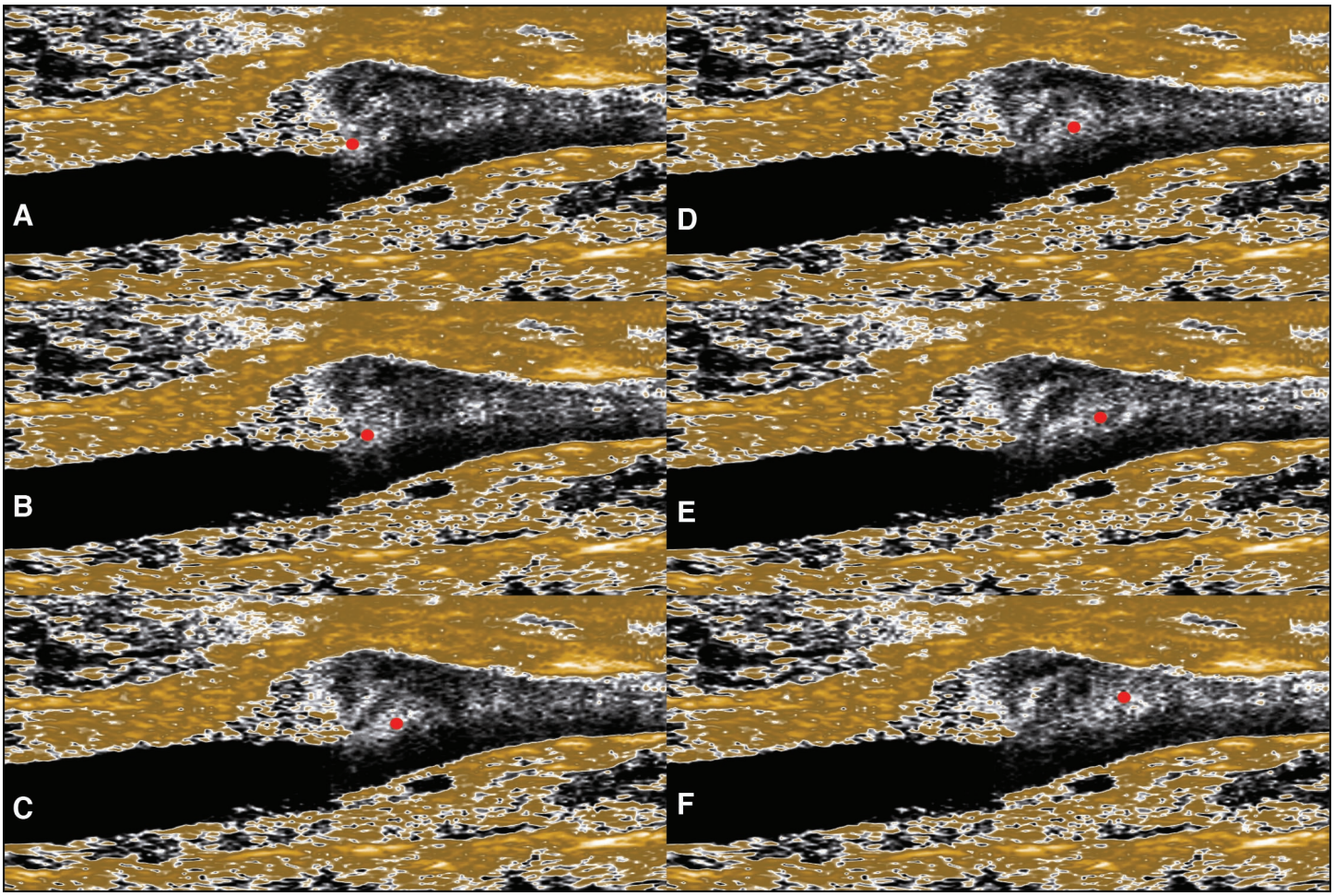

FIGURE 3. TIME SERIES OF THE DUS-EKV VISUALIZED FLOWS IN A MOUSE AAA MODEL. THE RED DOT INDICATES THE APPROXIMATE CENTER OF THE VORTEX. NOTE THE INITIAL FORMATION OF THE SEPERATION REGION (A) AND ITS DETACHMENT FROM THE WALL (B) FOLLOWED BY DISTAL MIGRATION (C-F). THE ENTIRE PROCESS OCCURS IN LESS THEN 1/15 OF THE CARDIAC CYCLE.

not surprisingly, the presence of the narrowing causes the separation to occur even earlier, almost immediately following the initial systolic acceleration of the flow. It is also pertinent to note that the presence of the narrowing causes the center of this vortex to be shifted towards the distal end of the aneurysm relative to the other two models at the time immediately prior to the peak systolic acceleration (Figure 5, first row). This highlights the increased momentum imparted to the intra-aneurysmal circulation by the presence of the narrowing, and the subsequent increase in the centerline velocity. These data suggest that the underlying cause of the observed vortex shedding is indeed shear-layer rollup, but the presence of a proximal lip or narrowing will decrease the velocity at which the proximal edge vortex separates.

Next, having determined the geometry was not the underlying cause of the vortex shedding, the role of the input flow-rate waveform was investigated. Three cases were explored, the case of steady flow, sine-wave driven flow (with a minimum velocity slightly greater then zero) and that of a carotid waveform (chosen with a peak-to-mean ratio of 1.6 as compared to the mouse waveform which had a value slightly greater then 3). Under steady flow conditions (Figure 6, first row), at a Reynolds number of 63, there was a single large recirculation zone within the aneurysm. For the Yip *et al*. [12] aneurysm and the case with the proximal lip this vortex was centered just above the aneurysm dome, while the proximal narrowing saw the center of the recirculation zone shifted towards the distal end of the aneurysm. When driven by the sine wave (Figure 6, third row) all three models were again seen to exhibit vortex shedding, showing a similar trend, as observed with the normal mouse waveform (Figure 6, second row) , of the proximal narrowing shedding at the onset of

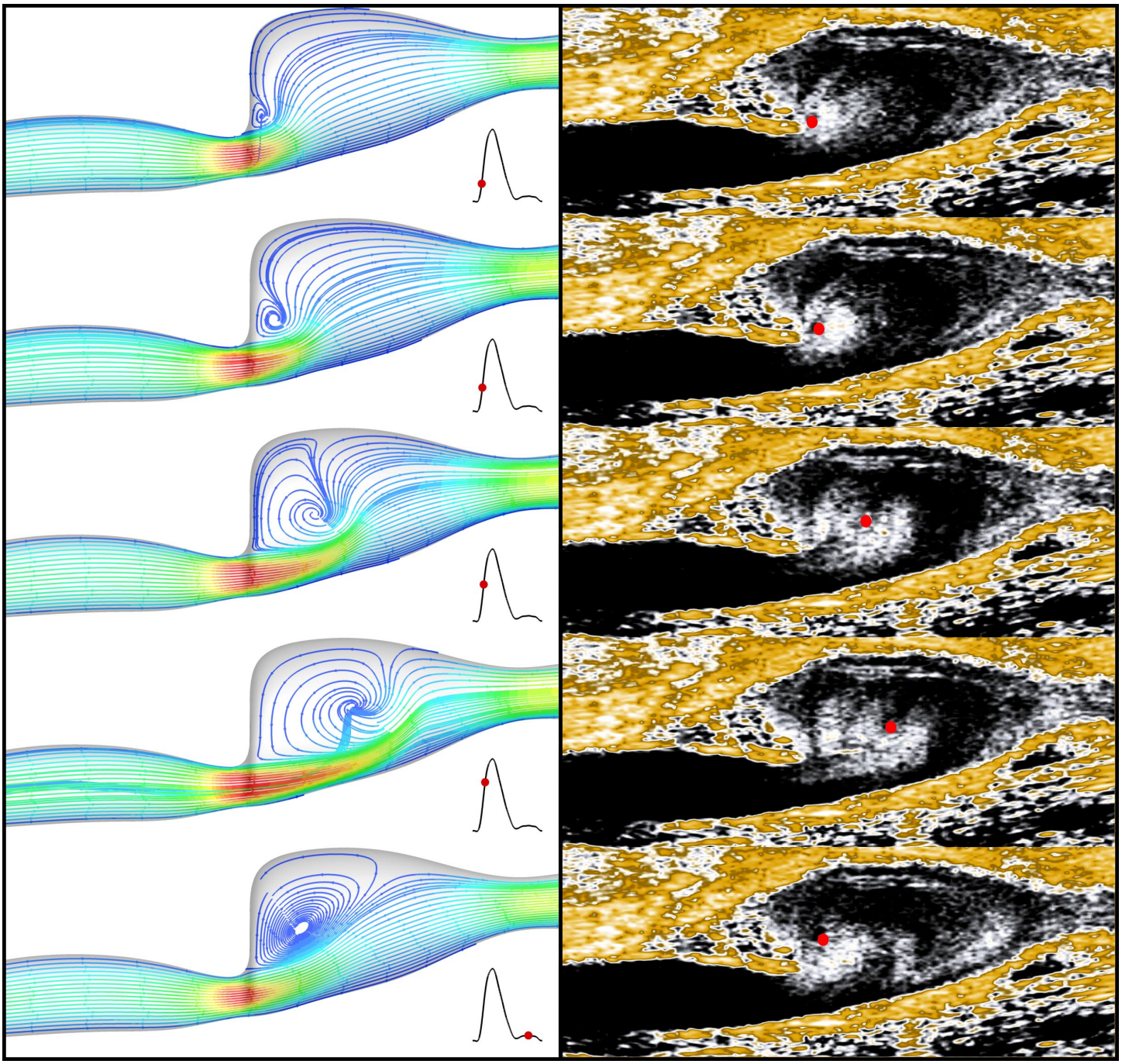

FIGURE 4. THE LEFT HAND COLUMN SHOWS THE VELOCITY STREAMLINES (COLOR CODED TO THE MAXIMUM VELOCITY AT EACH TIME POINT) FOR THE SEMI-IDEALIZED MOUSE MODEL. THE RIGHT HAND COLUMN SHOWS THE CORRESPONDING DUS-EKV IMAGE, NOTE THE DUS-EKV IMAGES WERE REGISTERED TO THE CFD DATA BY CHOOSING THE POINT OF VORTEX FORMATION AS THE INITIAL REGISTRATION POINT (IN TIME). THE RED DOT IN THE RIGHT HAND COLUM INDICATES THE APPROXIMATE CENTER OF THE VORTEX.

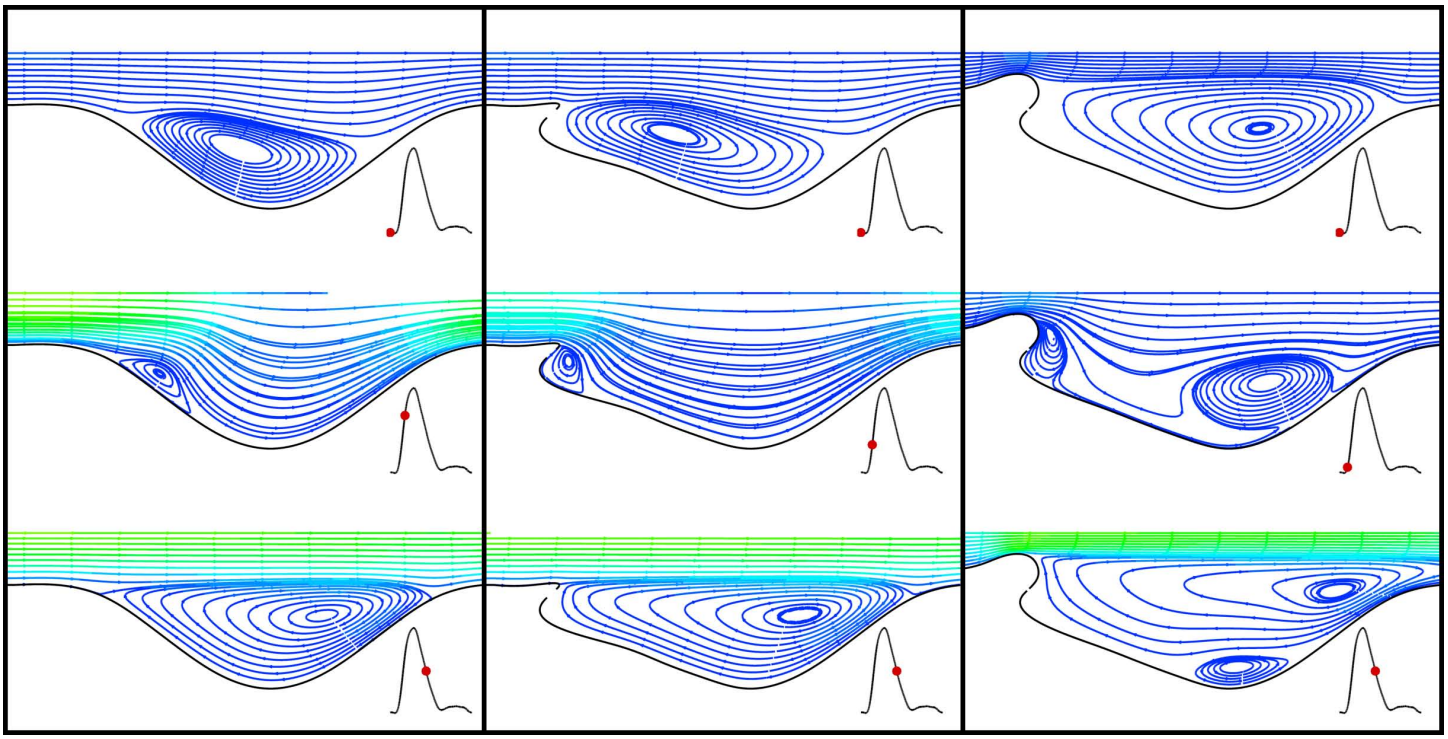

FIGURE 5. STREAMLINES COLOR-CODED TO THE MAXIMUM VELOCITY DURING THE CARDIAC CYCLE FOR THE THREE IDEALIZED GEOMETRIES; THE MODEL BASED ON YIP *et al*. [12] (LEFT COLUMN), THE PROXIMAL LIP (CENTRAL COLUMN) AND THE PROXIMAL NARROWING (RIGHT COLUMN).

the systolic rise followed by the proximal lip model and finally the Yip *et al*. [12] model exhibited shedding when the velocity exceeded the mean flow rate. The case of the carotid waveform (Figure 6, bottom row) was perhaps the most interesting as the Yip *et al*. [12] model and proximal lip model both exhibited vortex shedding following the similar trend of the proximal lip exhibiting shedding earlier in the systolic rise. However, the proximal narrowing model exhibited no shedding at any point in the cardiac cycle. This is attributed to the increased momentum imparted to the intra-aneurysmal vortex by the presence of the proximal narrowing (leading to a centerline velocity four times that of the other two models), and its increased momentum combined with the fact that flow rate never gets near zero (as in mouse and sine waveform) the shear layer never produces enough momentum to disrupt the large intra-aneurysmal circulation once it is set up leading to a single large vortex that is stable throughout the cardiac cycle.

DISCUSSION

This study has demonstrated the presence of a shear-layer rollup in the mouse AAA, which leads to vortex shedding from the proximal edge of the aneurysm to the distal end during the systolic acceleration phase of the cardiac cycle. This is assumed to be caused by the lower Reynolds number in the mouse, as compared to the human, causing the fluid in the aneurysm to be dragged along with the leading edge of the jet as it moves through the aneurysm. It is imperative to stress that this was first observed *in vivo* in the mouse AAA model, and CFD was used to investigate the mechanism by which this phenomenon was occurring. We have also demonstrated that the presence of a lip causes the separation to occur earlier during the systolic acceleration and, not surprisingly that, a proximal narrowing (leading to a higher velocity jet) leads to separation at the onset of systolic acceleration. We have further observed that under steady flow conditions the flow is characterized by a single large recirculation zone, with the center of the recirculation region shifted from the approximate center of the aneurysm to the distal end in the case of the proximal narrowing, attributed to the increased momentum of the central flow. The sine wave and carotid waveform inflow conditions have demonstrated that the vortex shedding is not entirely dependent on the shape of the inflow waveform. However the proximal narrowing model driven by the carotid waveform has shown that if the peak-to-mean ratio is small the momentum of the incoming fluid will not be sufficient to overcome the momentum of the intra-aneurysmal recirculation zone and cause vortex shedding to occur at the proximal edge.

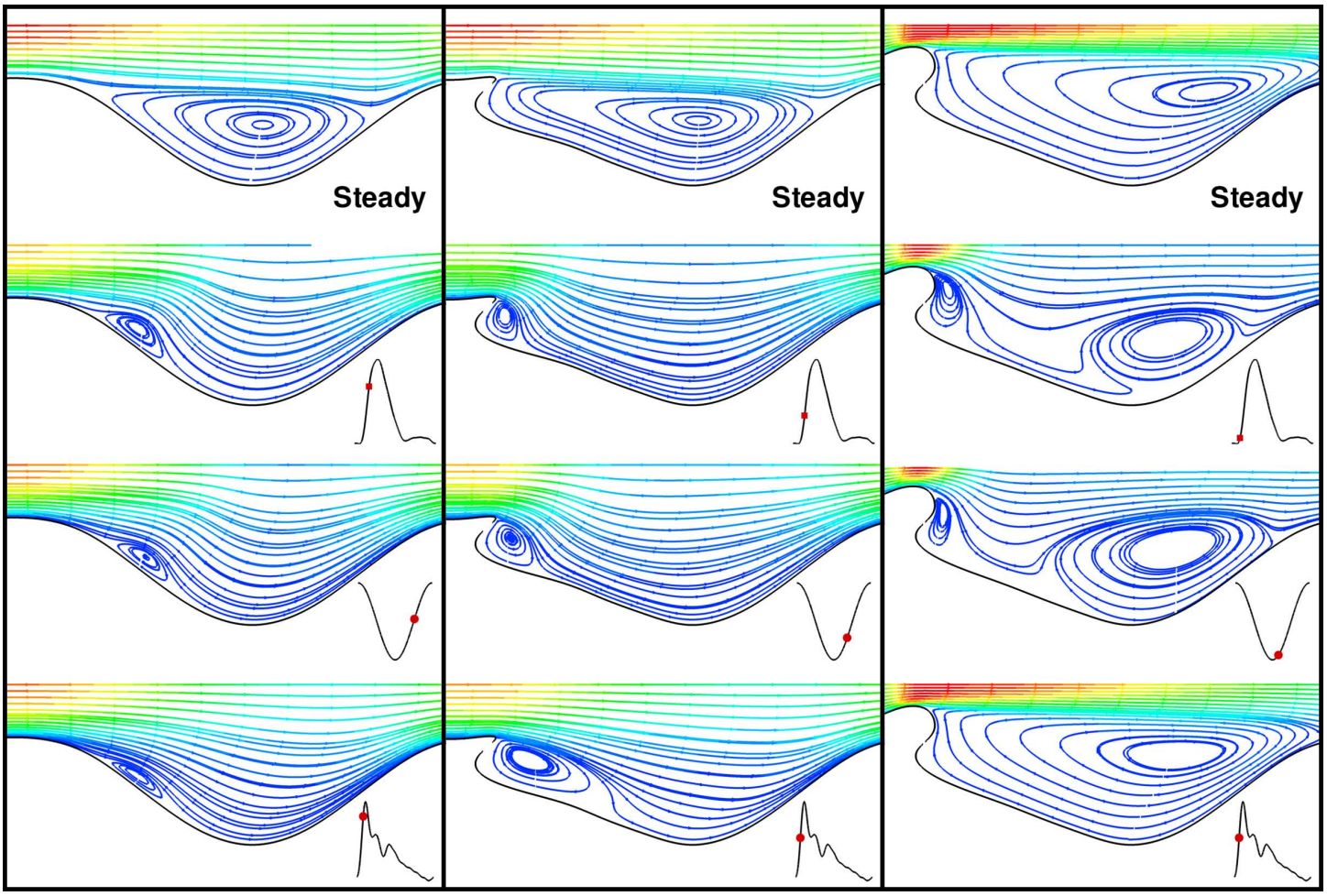

FIGURE 6. STREAMLINES (COLOR CODED TO THE MAXIMUM VELOCITY AT EACH TIME POINT) FOR THE YIP *et al*. [12] (LEFT COLUMN), PROXIMAL LIP (MIDDLE COLUMN) AND PROXIMAL NARROWING (RIGHT COLUMN) GEOMETRIES FOR THE CASES OF STEADY FLOW (TOP ROW) MOUSE WAVEFORM [20] (SECOND ROW), SINE WAVE (THIRD ROW) AND CAROTID WAVEFORM [21] (BOTTOM ROW).

A direct comparison, of our results, against the literature is not possible as there have been no previous studies investigating the the flow patterns in the mouse AAA. However, the DUS-EKV images show a high degree of correlation with the semi-idealized 3D model of the mouse AAA (Figure 4). It is of particular interest to note the differences in the fluid mechanics observed in this study with those of the human vasculature, as there has been much more extensive research done in this area. Previous studies investigating the human AAA fluid mechanics in idealized aneurysm models [11–15] have demonstrated the presence of a shed vortex from the proximal edge of the aneurysm during systolic deceleration. This is attributed to the fact that, as the fluid decelerates, it becomes unstable and a vortex forms and subsequently separates from the proximal edge. In comparison to this we have seen in the mouse AAA model that separation occurs during the systolic acceleration, and is attributed here to the vortex forming in the shear layer of the jet and subsequently being carried through the aneurysm by the momentum of the jet. During the systolic deceleration the flow consists of a single large recirculation zone and this recirculation zone persists through the diastolic tail of the cardiac waveform.

Although this paper has not focused on the biological implications of the observed flow, conjecture about the implications of the observed fluid mechanics on the life cycle of AAA. Figure 4 (bottom row) shows the fluid flow during the diastolic tail, which makes up roughly half of the cardiac cycle. This flow is dominated by the presence of a recirculation zone encompassing the upper proximal half of the aneurysm. What is interesting to note about the location of this recirculation zone is that this is the area in which the thrombus develops.

This study has required several simplifications and assumptions that should be mentioned here. As previously alluded to, a visually obvious limitation of this study is the lack of the animal-specific three-dimensional geometries. Although it would have been desirable to have such information, the present study has demonstrated that the vortex shedding is not entirely geometry dependent. The lack of a measured subject inflow waveform has required the use of the normal mouse suprarenal waveform [20], but again the flows we were studying were found not to be critically dependent on the waveform shape (at least with regards to using the animal-specific waveform versus a normal mouse waveform). Possibly the most critical limitation is the use of the rigid wall assumption for the mouse model. The B-mode images of the mouse AAA over the cardiac cycle showed the aneurysm itself to be relatively stationary, but the proximal abdominal aorta did show substantial deformation during the cardiac cycle.

CONCLUSION

Based on the data presented in this study we propose that the vortex shedding observed in the mouse model, during systolic acceleration, is unique to the mouse. Further geometric analysis of the mouse AAA combined with CFD studies will in future allow us to quantify more completely the fluid dynamic environment of the mouse AAA. It will also be necessary to look at the effects of scaling as the configuration changes from that of the mouse to the human, to understand further the cause of the shedding moving from the systolic acceleration in the mouse to the systolic deceleration in the human. The goal in future is to combine subject-specific mouse AAA CFD at various critical time points in the AAA development life cycle and look for links between the fluid dynamics and the evolution of the aneurysm. Even though the fluid mechanic environment between the mouse and the human may not be identical, the progression of the disease and its response to the fluid dynamics may have critical links to further our understanding of the human AAA life cycle.

ACKNOWLEDGMENT

MDF would like to thank NSERC for postdoctoral funding to complete this work. This work was made possible by the facilities of the Shared Hierarchical Academic Research Computing Network (SHARCNET:www.sharcnet.ca), Compute/Calcul Canada and the high performance computing virtual laboratory (HPCVL:www.hpcvl.org), Queen's University site. CDF was supported by CIHR grant MOP-93689, Heart and Stroke Foundation of Ontario Career Investigator Award (CI5960), the Canada Research Chairs program, Canadian Foundation for Innovation and Ministry of Research and Innovation Ontario.

REFERENCES

[1] Norman, P. E., and Powell, J. T., 2010. "Site specificity of aneurysmal disease". *Circulation,* ***121***(4), Feb, pp. 560–568.

[2] Golledge, J., Muller, J., Daugherty, A., and Norman, P., 2006. "Abdominal aortic aneurysm: pathogenesis and implications for management". *Arterioscler Thromb Vasc Biol,* ***26***(12), Dec, pp. 2605–2613.

[3] Isselbacher, E. M., 2005. "Thoracic and abdominal aortic aneurysms". *Circulation,* ***111***(6), Feb, pp. 816–828.

[4] Kuivaniemi, H., Platsoucas, C. D., and Tilson, M. D., 2008. "Aortic aneurysms: an immune disease with a strong genetic component". *Circulation,* ***117***(2), Jan, pp. 242–252.

[5] McCormick, M. L., Gavrila, D., and Weintraub, N. L., 2007. "Role of oxidative stress in the pathogenesis of abdominal aortic aneurysms". *Arterioscler Thromb Vasc Biol,* ***27***(3), Mar, pp. 461–469.

[6] Thompson, R. W., 2002. "Reflections on the pathogenesis of abdominal aortic aneurysms". *Cardiovasc Surg,* ***10***(4), Aug, pp. 389–394.

[7] Vorp, D. A., and Vande Geest, J. P., 2005. "Biomechanical determinants of abdominal aortic aneurysm rupture". *Arterioscler Thromb Vasc Biol,* ***25***(8), Aug, pp. 1558–1566.

[8] Daugherty, A., and Cassis, L. A., 2004. "Mouse models of abdominal aortic aneurysms". *Arterioscler Thromb Vasc Biol,* ***24***(3), Mar, pp. 429–434.

[9] Daugherty, A., Manning, M. W., and Cassis, L. A., 2000. "Angiotensin ii promotes atherosclerotic lesions and aneurysms in apolipoprotein e-deficient mice". *J Clin Invest,* ***105***(11), Jun, pp. 1605–1612.

[10] Daugherty, A., Rateri, D. L., and Cassis, L. A., 2006. "Role of the renin-angiotensin system in the development of abdominal aortic aneurysms in animals and humans". *Ann N Y Acad Sci,* ***1085***, Nov, pp. 82–91.

[11] Yu, S., 2000. "Steady and pulsatile flow studies in Abdominal Aortic Aneurysm models using Particle Image Velocimetry". *Int J Heat and Fluid Flow,* ***21***(1), FEB, pp. 74–83.

[12] Yip, T., and Yu, S., 2001. "Cyclic transition to turbulence in rigid abdominal aortic aneurysm models". *Fluid Dynamics Research,* ***29***(2), AUG, pp. 81–113.

[13] Taylor, T. W., and Yamaguchi, T., 1994. "Three-dimensional simulation of blood flow in an abdominal aortic aneurysm–steady and unsteady flow cases". *J Biomech Eng,* ***116***(1), Feb, pp. 89–97.

[14] Sheard, G. J., 2009. "Flow dynamics and wall shear-stress variation in a fusiform aneurysm". *J Eng Math,* ***64***(4), AUG, pp. 379–390.

[15] Finol, E. A., Keyhani, K., and Amon, C. H., 2003. "The effect of asymmetry in abdominal aortic aneurysms under physiologically realistic pulsatile flow conditions". *J Biomech Eng,* ***125***(2), Apr, pp. 207–217.

[16] Bluestein, D., Niu, L., Schoephoerster, R. T., and Dewanjee, M. K., 1996. "Steady flow in an aneurysm model: correlation between fluid dynamics and blood platelet deposition". *J Biomech Eng,* ***118***(3), Aug, pp. 280–286.

[17] Humphrey, J. D., and Taylor, C. A., 2008. "Intracranial and abdominal aortic aneurysms: similarities, differences, and need for a new class of computational models". *Annu Rev Biomed Eng,* ***10***, pp. 221–246.

[18] Les, A. S., Shadden, S. C., Figueroa, C. A., Park, J. M., Tedesco, M. M., Herfkens, R. J., Dalman, R. L., and Taylor, C. A., 2010. "Quantification of hemodynamics in abdominal aortic aneurysms during rest and exercise using magnetic resonance imaging and computational fluid dynamics". *Ann Biomed Eng,* ***38***(4), Apr, pp. 1288–1313.

[19] O'Rourke, M. J., and McCullough, J. P., 2008. "A comparison of the measured and predicted flowfield in a patient-specific model of an abdominal aortic aneurysm". *Proc Inst Mech Eng H,* ***222***(5), Jul, pp. 737–750.

[20] Amirbekian, S., Long, R. C., Consolini, M. A., Suo, J., Willett, N. J., Fielden, S. W., Giddens, D. P., Taylor, W. R., and Oshinski, J. N., 2009. "In vivo assessment of blood flow patterns in abdominal aorta of mice with mri: implications for aaa localization". *Am J Physiol Heart Circ Physiol,* ***297***(4), Oct, pp. 1290–1295.

[21] Ford, M. D., Alperin, N., Lee, S. H., Holdsworth, D. W., and Steinman, D. A., 2005. "Characterization of volumetric flow rate waveforms in the normal internal carotid and vertebral arteries". *Physiol Meas,* ***26***(4), Aug, pp. 477–488.

[22] Weller, H., Tabor, G., Jasak, H., and Fureby, C., 1998. "A tensorial approach to computational continuum mechanics using object-oriented techniques". *Computers in Physics,* ***12***(6), Nov/Dec, pp. 620–631.

[23] Womersley, J., 1955. "Method for the calculation of velocity, rate of flow and viscous drag in arteries when the pressure gradient is known". *J Physiol,* ***127***(3), pp. 553–563.